

This is an Open Access document downloaded from ORCA, Cardiff University's institutional repository:<https://orca.cardiff.ac.uk/id/eprint/114620/>

This is the author's version of a work that was submitted to / accepted for publication.

Citation for final published version:

Phillips, C. B., Hill, K. M., Paola, C., Singer, M. B. and Jerolmack, D. J. 2018. Effect of flood hydrograph duration, magnitude, and shape on bed load transport dynamics. *Geophysical Research Letters* 45 (16) , pp. 8264-8271. 10.1029/2018GL078976

Publishers page: <http://dx.doi.org/10.1029/2018GL078976>

Please note:

Changes made as a result of publishing processes such as copy-editing, formatting and page numbers may not be reflected in this version. For the definitive version of this publication, please refer to the published source. You are advised to consult the publisher's version if you wish to cite this paper.

This version is being made available in accordance with publisher policies. See <http://orca.cf.ac.uk/policies.html> for usage policies. Copyright and moral rights for publications made available in ORCA are retained by the copyright holders.



23 **Abstract**

24 Bed load sediment transport is an inherently challenging process to measure within a river,
25 which is further complicated by the typically transient nature of the hydrograph. Here we use
26 laboratory experiments to explore how sediment flux under transient – unsteady and intermittent
27 – flow differ from those under steady flow. For a narrow unimodal sediment distribution, we
28 calculated fluid stress and measured sediment flux for a range of hydrograph durations,
29 magnitudes, shapes, and sequences. Within a hydrograph, we find considerable variability in
30 sediment flux for a given stress above the threshold for motion. However, cumulative bed-load
31 flux resulting from a flood scales linearly with the integrated excess transport capacity (flow
32 impulse). This scaling indicates that, to first order, flow magnitude, duration, shape, and
33 sequence are only relevant to bedload flux in terms of their contribution to the total flow
34 impulse, in agreement with prior field results. The flood impulse represents a quantitative
35 parameter through which the effects of transient flow on coarse sediment transport may be
36 parsed.

37

38 **Plain language summary**

39 Mountain river floods produced from snowmelt can last months but remain relatively shallow,
40 while floods resulting from storms are often shorter in duration and deeper. These floods have, in
41 a sense, different “shapes” and “sizes” determined by their environment and climate. We
42 performed laboratory experiments to understand how these flood shapes and sizes affect the
43 amount of sediment they can move, a key precursor to understanding how rivers and flooding
44 impact the landscapes in which they reside. Our experiments show that if one accounts for the
45 forcing of the flood in a physically based manner, there is no difference between floods of
46 different shapes and sizes in terms of how much sediment they move. We suggest that these
47 results may make floods easier to characterize when modeling landscapes.

48

49 **1. Introduction**

50 Under steady flow, the rate of bed-load transport in rivers is a stochastic process that varies both
51 spatially and temporally due to turbulent fluid-stress fluctuations, bed topography, and granular
52 structure. Field and laboratory observations demonstrate that variability within the grain size
53 distribution (Wilcock and McArdell, 1997), the magnitude of upstream sediment supply (Singer,

54 2010; Recking, 2012), mobility (Wilcock, 1998), and structural arrangement (Church et al.,
55 1998; Strom et al., 2004; Zimmermann et al., 2010; Marquis and Roy, 2012; Houssais et al.,
56 2015) of river-bed sediments affect the flux resulting from an applied flow stress (Recking,
57 2013). Stream hydrology is assumed to be a primary control on the magnitude and duration of
58 the applied bed stress. In natural environments, river flows are rarely steady as gravel-bed rivers
59 typically experience flows that exceed the threshold required for sediment motion only during
60 floods. Strictly speaking, natural floods violate the assumptions of steady and uniform flow
61 required for current sediment transport calculations. The transience of natural hydrographs
62 presents a barrier to applying the mechanistic understanding of sediment transport dynamics
63 developed under steady flows in laboratory experiments to natural rivers.

64
65 At timescales of a single flood event (from the initiation of motion to the cessation of bed
66 material transport) to timescales of multiple flood events, it remains an open question how steady
67 and transient flows differ in terms of their effects on channel morphology and bed load sediment
68 dynamics. Observations within the natural environment have led to the attribution of various
69 phenomena to aspects of transient flow such as: the degree of vertical and spatial bed grain size
70 segregation (armor) (Reid and Laronne, 1995), the amount of grain protrusion (Yager et al.,
71 2012), channel bed complexity (Singer and Michaelides, 2014; Whiting and Stamm, 1995), and
72 variability in the threshold of motion (Turowski, 2011). However, for flows in natural rivers it is
73 exceedingly difficult to distinguish between phenomena that occur under steady flow and those
74 that require a transient hydrograph. The majority of transient-flow laboratory experiments
75 explore the role of magnitude and duration (Hassan et al., 2006; Bombar et al., 2011; Humphries
76 et al., 2012; Mao, 2012), flow sequence (Humphries et al., 2012; Guney et al., 2013; Waters and
77 Curran 2015), and to a lesser degree the time between floods (intermittency) (Ferrer-Boix and
78 Hassan, 2015; Masteller and Finnegan, 2017) on the development of bed-surface texture in
79 mixed unimodal or bimodal sediment beds. When compared with their accompanying steady
80 flow counterparts, these experiments collectively paint a complex picture of the intermixing of
81 gravel-bed morphology, adjustment timescales, and mixed grain-size mobility thresholds (e.g.
82 Wilcock, 1998; Wilcock and Crowe, 2003; Parker et al. 2008) with changing flow rates at
83 various durations. Using a well sorted gravel sediment with constant sediment feed and a
84 sequence of identical hydrographs, Wong and Parker (2006) determined that downstream of a

85 short inlet boundary layer, the sediment flux adjusted to track the variations in the hydrograph.
86 The use of sediment beds with broad, mixed, or bimodal grain-size distributions complicates
87 these findings considerably (An et al., 2017). With more complex grain-size distributions the
88 magnitude of the peak and duration of the rising and falling limbs have the potential to create
89 bed states with a higher threshold of motion (Mao, 2012). These complex bed states induce a
90 variety of hysteresis loops between flow and sediment flux (Mao, 2012; Humphries et al., 2012;
91 Guney et al., 2013), making it difficult to predict the instantaneous flux using equations
92 developed under steady flow conditions (Guney et al., 2013; Lee et al., 2004). However, despite
93 the shortcomings of most transport equations to compute instantaneous transport, they can be
94 modified to provide reasonable predictions of the total flux (Lee et al., 2004; Wong and Parker,
95 2006; Humphries et al., 2012), suggesting that this complexity may not be intractable over
96 complete flood hydrographs.

97
98 Linking sediment transport dynamics to landscape evolution requires developing physically
99 based metrics capable of bridging the gaps between discrete floods, sequences of hydrographs
100 that define a regional climate, and the long-term approximation of hydrographs within landscape
101 evolution models (Paola et al., 1992; Lague, 2014; Phillips and Jerolmack, 2016). Recent field
102 results on the transport of marked tracer cobbles demonstrate that despite substantial hydrologic
103 variability, average particle displacement scales linearly with the integrated excess shear
104 velocity, or impulse (Phillips et al., 2013; Phillips and Jerolmack, 2014; Imhoff and Wilcox,
105 2016), suggesting that to first order the effects of flow transience may be accounted for through
106 the quantification of the flow impulse. However, substantial variability exists within these data
107 as the cumulative impulse is scaled down to that of a single flood. Here we report results from
108 laboratory flume experiments at St. Anthony Falls Laboratory (SAFL) at the University of
109 Minnesota under transient flow to quantitatively compare the flow impulse to bed load flux for
110 individual floods and sequences of floods (Phillips, 2018). These experiments explore a
111 parameter space of magnitude and duration for four geometrically simplified flood shapes. We
112 demonstrate that even with a well sorted unimodal sediment bed, there is considerable variability
113 in instantaneous flux-stress relationships for different flood shapes. At the same time, we show
114 that, when integrated over a flood hydrograph, flows of equivalent total impulse transport the

115 same total sediment flux. Finally, we show how the impulse concept can be used to normalize
 116 floods to facilitate the comparison of both steady and unsteady floods.

117

118 **2. Experiments**

119 **2.1 Experimental design**

120 Our experiments do not attempt to recreate a natural flood regime in the lab (Paola et al., 2009).

121 Rather they are designed to understand how transport in transient flows might differ from steady

122 flows and how the components of transient flows, unsteadiness and intermittence, potentially

123 contribute to different sediment dynamics. We explore these components of flow transience

124 through the use of sequences of geometrically simplified steady and unsteady floods where the

125 effects of flood peak magnitude, duration, and shape on sediment transport dynamics can be

126 independently investigated (Figure 1a-b). For clarity, in this Letter, we use the term ‘flood’ to

127 refer to a distinct transport event, from the period where particles start moving to when they stop.

128 We use ‘flood shape’ to describe the time dependence of the flow magnitude for a single flood,

129 and the phrase ‘flood sequence’ to refer to multiple sequential discrete floods. Flood sequences

130 of steady or unsteady floods represent the intermittent component of transient flows (Figure 1c).

131 To compare the effects of these components on particle transport, we normalize each flood by its

132 potential fluid-derived transport capacity, or impulse (T_*):

$$133 T_* = \int_{t_s}^{t_f} (U_\tau^2 - U_{\tau c}^2)^{3/2} dt / gD^2 \quad (1)$$

134 where U_τ is the shear velocity (m/s), $U_{\tau c}$ is the threshold shear velocity for sediment motion

135 (m/s), g is the acceleration due to gravity (m/s^2), D is a representative grain size (m) taken here

136 as the geometric mean, and t_f and t_s are the starting and ending times of the flood, respectively.

137 We note that equation (1) is valid only for flows able to transport sediment ($U_\tau > U_{\tau c}$). We then

138 compare runs of equivalent T_* and varying magnitude, duration, and shape in terms of their

139 measured dimensionless cumulative sediment flux (Q_*):

$$140 Q_* = \int_{t_s}^{t_f} (q_b) dt / D^2 \quad (2)$$

141 where q_b is the volumetric sediment flux per unit width (m^2/s). Normalizing each flood by T_*

142 accounts for the expected average behavior under steady flow, effectively representing all flows

143 as square waves, because T_* does not distinguish between flow magnitude, duration, or shape.

144

145 We performed two experiments to isolate the effects of transient flow at the flood scale. The first
146 experiment is comprised of sequences of floods with constant peak hydrograph magnitudes,
147 while sequences of floods in the second experiment had variable peak magnitudes (Figure 1c). In
148 the first type of experiments, we ran sequences (12-20) of intermixed steady and unsteady floods
149 with equal T^* and equivalent hydrograph peak magnitude. To explore a parameter space of peak
150 magnitude and duration (Figure 1b) we ran additional sequences with increased or decreased
151 flood magnitude and/or flood duration (see supporting information and Figure S2). The second
152 set of experiments was designed to test the effects of sequences of floods (6-12) with variable
153 magnitude and duration (Figure 1c lower panel). These experiments allow us to contrast sets of
154 floods with high magnitude and short duration against those of low magnitude and longer
155 duration, but with equivalent T^* . Throughout both experiments, the bed within the test section of
156 the flume was not disturbed or altered; it was allowed to evolve.

157

158 **2.2 Experimental setup**

159 We conducted the experiments at SAFL in a 30 m by 0.5 m sediment and water feed flume
160 (Figure S1). Water discharge (Q , m³/s) was controlled using a variable speed pump that
161 discharged into a head tank before flowing over a weir and entering the 22.5 m long
162 experimental section of the flume. The flume data acquisition system was set up to record
163 measurements every second of water surface elevation and the mass of sediment accumulating at
164 the end of the flume. A narrow unimodal mixture of sediment (with geometric mean diameter
165 $D=7.2$ mm and standard deviation 1.2 mm) was fed 2.5 m downstream of the inlet weir via
166 sediment feeder during all periods when bed shear stress exceeded the critical threshold for
167 motion. We note that we used the same sediment and flume, though with a different setup, as
168 used in Wong and Parker (2006), Wong et al. (2007), and Hill et al. (2010). For each run, water
169 discharge was brought from baseflow up to the peak flow rate and then back to baseflow. In the
170 case of unsteady runs, the rate of rise and fall depends on the shape of the hydrograph (Figure 2a
171 & S2). This results in a temporally variable and often rapidly changing flow depth within the
172 flume. We kept the slope of the sediment bed at steady state, no net aggradation or erosion, by
173 feeding sediment for each flood such that $Q_{*in} \approx Q_{*out}$, resulting in a proportional feed system. To
174 achieve this, we adjusted the sediment feed rate for each flood (Figure S3) such that sediment

175 was supplied only during periods where the flood was capable of transporting sediment (see
 176 supporting information for additional details).

177
 178 Cumulative time series of sediment mass leaving the flume were continuously recorded as the
 179 sediment deposited in a submerged suspended basket attached to a load cell (Interface SMT2-
 180 500 N load cell, Figure S1). Water surface elevation (1 Hz, 1 mm accuracy) was measured at
 181 three locations within the flume using ultrasonic transducers (Massa mPulse M-5000, Figure S1).
 182 To reduce experimental noise within the time series all data were smoothed using a Savitzky-
 183 Golay filter (7 second window, 2nd order polynomial). Laser sheet scans of bed topography (1
 184 mm vertical and horizontal accuracy) were taken between sets of floods after the flow was turned
 185 off and the flume had been allowed to drain the surface layer. The sediment mass, bed
 186 topography scans, and water surface elevation data were used to derive the remaining variables.
 187 Sediment flux (q_s , kg/s) represents the derivative of the cumulative mass time series over an
 188 eight-second moving window. Water surface slope (S) was estimated from the first and third
 189 sensors by linear regression (see supporting information for further explanation). Flow depth (h ,
 190 m) was estimated by differencing the intermittent bed topography scans from the water surface
 191 elevation time series. The sediment bed slope remained relatively constant ($S_{mean}=9.3\times 10^{-3}$ and
 192 $S_{SD}=7.4\times 10^{-4}$) throughout both series of experiments, and differences in bed elevation (ΔZ , mm)
 193 between scans for the location where h was calculated were small ($\Delta Z_{mean}=-0.1$ mm and
 194 $\Delta Z_{SD}=1.5$ mm). Flow velocity (U , m/s) was calculated as $U=Q/(hb)$ where b is the flume width.
 195 Shear stress (τ , Pa) was approximated using the procedure outlined in Vanoni and Brooks (1975)
 196 to account for sidewall effects using time series of: h , S , Q , and U . We calculated shear velocity
 197 as $U_\tau = \sqrt{\tau/\rho}$ and Shields stress as $\tau_* = \tau/(\rho_s - \rho)gD$, where ρ_s is sediment density (2650
 198 kg/m³), and ρ is the water density. Additional methodological notes are available in the
 199 supporting information.

200

201 **3. Results**

202 For each flood, measured time series of water surface elevation and sediment mass were used to
 203 derive time series of flow discharge, velocity, depth, water surface slope, and sediment flux
 204 (Figure 2). Time series data are available for 209 runs totaling 23.5 hours of experiments and
 205 2,155 kg of transported sediment with: peak $U_\tau=0.087-0.12$ ($\tau_*=0.065-0.12$), ratios of peak

206 $U_{\tau}/U_{\tau_c}=1.08-1.5$ ($\tau^*/\tau_{*c}=1.18-2.23$), total durations ranging from 2.5-30 min, durations above the
 207 threshold of motion of 0.6-29.1 min (Figure 1c), and cumulative flux masses per flood ranging
 208 from 1-32 kg. We examine the results from these experiments first within individual floods and
 209 second at the scale of a complete flood and multiple flood sequences.

210

211 **3.1 Within a flood**

212 Within each flood there is considerable variability between sediment flux and stress; however we
 213 find that to first order the stress flux data can be described by a bed-load transport equation of the
 214 form $q^*=K(\tau^*-\tau_{*c})^\alpha$ (Meyer-Peter and Müller, 1948; Wong and Parker, 2006) (Figure 2b), where
 215 q^* is the dimensionless volumetric sediment flux. Here we fix the exponent at $\alpha=1.5$ (Wong and
 216 Parker, 2006; Wong et al., 2007). Allowing α to vary produces only minor improvements that do
 217 not provide a strong justification for the additional free parameter. We note that similar
 218 formulations of the flux law (see Table 1 in Lajeunesse et al., 2010) provide equally convincing
 219 fits to the data. For any given run, we observe a small range of coefficients, average threshold
 220 stresses, and in some cases thresholds of initiation and cessation of transport (Figure 2b & c) that
 221 change between rising and falling hydrograph limbs. We observe counter-clockwise hysteresis in
 222 sediment flux primarily when the flow changes rapidly. The hysteresis occurs over short
 223 timescales and represents a small fraction of the sediment flux. Hysteresis in sediment flux and
 224 hysteresis in the threshold of motion were not always coincident in the same flood.

225

226 **3.2 Flood and sequence scale**

227 Examining the flux data at the sequence scale we find that all steady and transient floods follow
 228 a similar trend (Figure 3a). There is considerable scatter in the flux data; however, the mean of
 229 the data cloud is well described by a single transport law of the same power law form fit to data
 230 from individual floods (Figure S4a), except those at the highest stresses, where data are sparse.
 231 We fit the transport law to all data where $q^* \geq 0$ and $\tau^* \geq 0.045$ by least-squares regression,
 232 yielding parameters for the coefficient ($K=5.0$) and threshold of motion ($\tau_{*c}=0.055$). These
 233 cutoffs for τ^* and q^* arise from the sensitivity of the load cell and noise associated with the
 234 experimental set up of the sediment weighing basket. We also separated the bulk flux data into
 235 steady and unsteady floods as well as by flood shape to assess if these subsets of the data
 236 behaved differently. Inspection of the distributions of residuals determined from the transport

237 law (fit in Figure 3a) for each subset yield minimal discernable differences between them (Figure
238 S4a-c).

239
240 To compare flows of different shape, peak magnitude, and duration we computed T^* for each
241 flood (eq. 1). Since the flux data can be represented with a single transport law (Figure 3a), we
242 compute equations 1 and 2 for all runs using a single value for the threshold of motion ($U_{\tau c}=0.08$
243 m/s). Additionally, we use a single value for grain size ($D=0.0072$ m) in both equations 1 and 2.
244 After computing both integrated parameters we find that to first order the T^* parameter collapses
245 the flux data onto a single linear trend (Figure 3b). All floods but one are within a factor of 1.5 of
246 the mean trend. Within this data collapse, there is no systematic variation in the data with respect
247 to flood magnitude, duration, or shape.

248

249 **4. Discussion and Conclusions**

250 The degree of complexity present in the flux data for each run (Figure 2 a-c) is evident in the
251 hysteresis present in both the calculated threshold of motion and magnitude of flux on the rising
252 and falling limbs of unsteady flows. Hysteresis loops in these experiments occur for floods with
253 rapidly changing hydraulic stresses and are typically absent in runs when the flow gradually
254 increases or decreases. The short timescales over which the hysteresis is present for both rising
255 and falling flows indicate a lag between the calculated instantaneous stress via the depth-slope
256 product and the response of the bed, suggesting there may be a minimum time required to
257 average the flow conditions in order to compute a representative stress via the depth-slope
258 product. Hysteresis is common in transient flow experiments (Hassan et al., 2006; Mao, 2012),
259 however the short run times and well-sorted gravel bed presented here preclude most of the
260 commonly reported mechanisms. The narrow grain size distribution reduces grain scale sorting,
261 armoring, and size selective transport, which even under steady flows can result in differentially
262 mobile populations of bed sediments (Wilcock and McArdell, 1997). Additionally, the short
263 duration of competent flow limits the effects of phenomena with longer timescales of adjustment
264 such as bedforms and sediment texture (Ferrer-Boix and Hassan, 2014). In terms of total flux,
265 though, the observed hysteresis represents a small fraction of the sediment transported in a flood.

266

267 Interestingly, and perhaps surprisingly, this intra-flood variability is not evident at the scale of a
268 single flood, in which T^* collapses the Q^* data onto a single linear relation (Figure 3b). In terms
269 of their cumulative sediment flux, the linear scaling between T^* and Q^* indicates that unsteady
270 runs are equivalent to steady runs. The scatter in cumulative flux about the mean trend does not
271 vary systematically with flood duration, peak magnitude, shape, or sequence, indicating its
272 source is not associated with flood type or flow transience. Additionally, the data collapse
273 indicates that for the parameter space explored here, flow magnitude and duration are relevant
274 only in how they contribute to T^* . Under these conditions the sediment flux does not depend on
275 the flow history, indicating that the sequence of runs did not exert substantial control on the total
276 flux. This flow history independence indicates a memoryless system under the given conditions.
277 In terms of flood intermittency, the linear scaling indicates that not only can a series of smaller
278 events' impulses be summed to equal a run with a larger impulse, but that the sequence of the
279 smaller impulses of various shapes does not matter (Figure 1 & 3).

280

281 The linear scaling between T^* and Q^* and its implications are contingent on the validity of the
282 non-linear flux law relating U_τ or τ^* to q^* that forms the basis of the impulse (Equation 1).
283 However, these experiments demonstrate that this relation need be valid only at an integral scale
284 to recover a reasonable collapse of the data (Figure 3b), though this integral scale remains to be
285 determined in natural systems. To place these results into a broader context, we summarize two
286 important limitations of these experiments: (1) limited flow durations and (2) limited range of
287 shear velocity. The limited flow durations simulated here preclude the observation of
288 morphologic structures with longer time scales of formation or adjustment, if they are not
289 already precluded by the narrow grain size distribution. The range in peak stress magnitudes is
290 comparable to previous similar experiments (Hassan et al., 2006; Mao, 2012; Humphries et al.,
291 2012) and represents approximately half the reach average transport capacity ($U_\tau/U_{\tau c}$) observed
292 within natural bed load rivers (Phillips and Jerolmack, 2016). In practice, this limited range of
293 peak stresses may be less restricting as bed-load flux laws are more robust for $U_\tau \gg U_{\tau c}$ (Capart
294 and Fraccarollo, 2011; Recking et al., 2012). Meaningful deviations from the flux law are more
295 likely for floods with low stress magnitudes near the threshold of motion, where sufficiently
296 longer averaging timescales are required (Recking et al., 2012; Houssais et al., 2015). In such
297 cases, dynamic interactions between the bed and the flow may be capable of altering $U_{\tau c}$. This

298 includes processes such as bed dilation due to high stresses or compaction from constant forcing
299 above and below the threshold of motion (Charru et al. 2004; Marquis and Roy, 2012; Houssais
300 et al., 2015; Masteller and Finnegan, 2017). However, such dynamic interactions were not
301 observed within the data.

302
303 The largest unknown is the role of the grain size distribution, as the narrow one used here greatly
304 reduced the textural, morphological, and granular adjustments that could have occurred (see
305 Ferrer-Boix and Hassan, 2014) within the flume (by design). Introducing a wider grain-size
306 distribution with particle size dependent mobility (common for broad or bimodal grain size
307 distributions) would likely require the impulse in equation (1) to be modified to reflect a
308 fractional transport equation (Wilcock and Crowe, 2003). The narrow grain size distribution was
309 chosen to isolate the influence of the hydrograph; however, one of the implications of our
310 experiments is that the grain-size distribution potentially represents the largest source of
311 variability (Hassan et al., 2006). It remains an open question which grain-size distribution
312 (bimodal, broad, or mixed transport), when paired with transient flow, has the greatest potential
313 to add memory to the system.

314
315 Despite the limitations, our results may be more general than they initially seem. These
316 experiments support the surprising conclusion that the total sediment mass transported is
317 insensitive to the details of the transient hydraulic forcing, as has also been observed for bed load
318 tracers in natural rivers (Phillips et al., 2013; Imhoff and Wilcox, 2016). Additionally, these
319 results are (in spirit) the same treatment of the hydrograph embodied in the simplest physically
320 based models of landscape evolution (see Paola et al., 1992), where the full complexity of a
321 hydrograph is replaced by the bankfull flood (average, see Phillips and Jerolmack, 2016)
322 multiplied by an intermittency factor. This similarity is by no means a complete test of such
323 treatments, due to our simplified size distribution, other missing processes, and scale differences,
324 yet it does reinforce the notion present in both landscape evolution models and field tracer
325 studies that substantial complexity need not preclude a simple treatment.

326

327 **Acknowledgements**

328 Research was supported by a NSF-Postdoctoral Fellowship (EAR-1349776), the National Center
329 for Earth Surface Dynamics 2 (NCED2, EAR-1246761), and the NSF INSPIRE program (EAR-
330 1344280). We thank S. Harrington and K. Francois-King for outstanding laboratory assistance.
331 These experiments were performed at St. Anthony Falls Laboratory and benefitted from the
332 technical support of: C. Ellis, R. Gabrielson, E. Steen, B. Erickson, and R. Christopher. We
333 thank L. Hsu and J. Myers for assistance with data publication. Finally, we thank S. Chartrand
334 and an anonymous reviewer for comments that increased the clarity of this manuscript.
335 Experimental data and processing codes are publicly available through the SEAD repository
336 (<http://doi.org/10.5967/MOS180MK>).

337

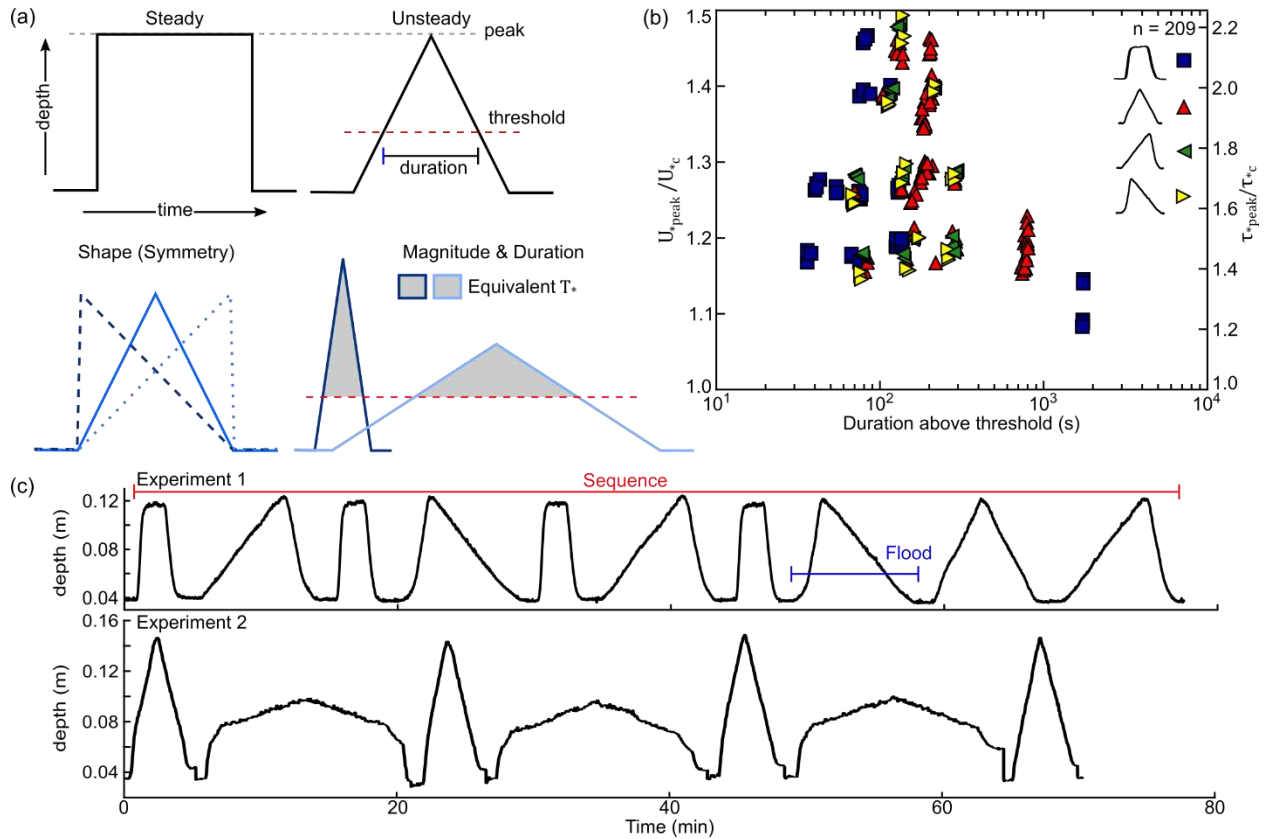
338 **References**

- 339 An, C., Fu, X., Wang, G., & Parker, G. (2017). Effect of grain sorting on gravel bed river
340 evolution subject to cycled hydrographs: Bed load sheets and breakdown of the
341 hydrograph boundary layer. *Journal of Geophysical Research: Earth Surface*, 122(8),
342 2016JF003994. <https://doi.org/10.1002/2016JF003994>
- 343 Bombar, G., Elci, S., Tayfur, G., Guney, S., & Bor, A. (2011). Experimental and Numerical
344 Investigation of Bed-Load Transport under Unsteady Flows. *Journal of Hydraulic
345 Engineering-Asce*, 137(10), 1276–1282. [https://doi.org/10.1061/\(ASCE\)HY.1943-
346 7900.0000412](https://doi.org/10.1061/(ASCE)HY.1943-7900.0000412)
- 347 Capart, H., & Fraccarollo, L. (2011). Transport layer structure in intense bed-load. *Geophysical
348 Research Letters*, 38(20), L20402. <https://doi.org/10.1029/2011GL049408>
- 349 Charru, F., Mouilleron, H., & Eiff, O. (2004). Erosion and deposition of particles on a bed
350 sheared by a viscous flow. *Journal of Fluid Mechanics*, 519, 55–80.
351 <https://doi.org/10.1017/S0022112004001028>
- 352 Church, M., Hassan, M. A., & Wolcott, J. F. (1998). Stabilizing self-organized structures in
353 gravel-bed stream channels: Field and experimental observations. *Water Resources
354 Research*, 34(11), 3169–3179. <https://doi.org/10.1029/98WR00484>
- 355 Ferrer-Boix, C., & Hassan, M. A. (2014). Influence of the sediment supply texture on
356 morphological adjustments in gravel-bed rivers. *Water Resources Research*, 50(11),
357 8868–8890. <https://doi.org/10.1002/2013WR015117>
- 358 Ferrer-Boix, C., & Hassan, M. A. (2015). Channel adjustments to a succession of water pulses in
359 gravel bed rivers, *Water Resources Research*, 51, 8773–8790,
360 [doi:10.1002/2015WR017664](https://doi.org/10.1002/2015WR017664).
- 361 Guney, M. S., Bombar, G., & Aksoy, A. O. (2013). Experimental Study of the Coarse Surface
362 Development Effect on the Bimodal Bed-Load Transport under Unsteady Flow
363 Conditions. *Journal of Hydraulic Engineering*, 139(1), 12–21.
364 [https://doi.org/10.1061/\(ASCE\)HY.1943-7900.0000640](https://doi.org/10.1061/(ASCE)HY.1943-7900.0000640)
- 365 Hassan, M. A. & Church, M. (2000). Experiments on surface structure and partial sediment
366 transport on a gravel bed. *Water Resources Research*, 36, 1885-1895,
367 doi.org/10.1029/2000WR900055

- 368 Hassan, M. A., Egozi, R., & Parker, G. (2006). Experiments on the effect of hydrograph
 369 characteristics on vertical grain sorting in gravel bed rivers. *Water Resources Research*,
 370 42, 15. <https://doi.org/200610.1029/2005WR004707>
- 371 Hill, K. M., DellAngelo, L., & Meerschaert, M. M. (2010). Heavy-tailed travel distance in gravel
 372 bed transport: An exploratory enquiry. *Journal of Geophysical Research*, 115, F00A14.
 373 <https://doi.org/10.1029/2009JF001276>
- 374 Houssais, M., Ortiz, C. P., Durian, D. J., & Jerolmack, D. J. (2015). Onset of sediment transport
 375 is a continuous transition driven by fluid shear and granular creep. *Nature*
 376 *Communications*, 6, 6527. <https://doi.org/10.1038/ncomms7527>
- 377 Humphries, R., Venditti, J. G., Sklar, L. S., & Wooster, J. K. (2012). Experimental evidence for
 378 the effect of hydrographs on sediment pulse dynamics in gravel-bedded rivers. *Water*
 379 *Resources Research*, 48, 15. <https://doi.org/201210.1029/2011WR010419>
- 380 Imhoff, K. S., & Wilcox, A. C. (2016). Coarse bedload routing and dispersion through tributary
 381 confluences. *Earth Surface Dynamics*, 4(3), 591–605.
 382 <https://doi.org/https://doi.org/10.5194/esurf-4-591-2016>
- 383 Lague, D. (2014). The stream power river incision model: evidence, theory and beyond. *Earth*
 384 *Surface Processes and Landforms*, 39(1), 38–61. <https://doi.org/10.1002/esp.3462>
- 385 Lajeunesse, E., Malverti, L., & Charru, F. (2010). Bed load transport in turbulent flow at the
 386 grain scale: Experiments and modeling. *Journal of Geophysical Research*, 115, 16.
 387 <https://doi.org/201010.1029/2009JF001628>
- 388 Lee, K. T., Liu, Y.-L., & Cheng, K.-H. (2004). Experimental investigation of bedload transport
 389 processes under unsteady flow conditions. *Hydrological Processes*, 18(13), 2439–2454.
 390 <https://doi.org/10.1002/hyp.1473>
- 391 Mao, L. (2012). The effect of hydrographs on bed load transport and bed sediment spatial
 392 arrangement. *Journal of Geophysical Research-Earth Surface*, 117.
 393 <https://doi.org/10.1029/2012JF002428>
- 394 Marquis, G. A., & Roy, A. G. (2012). Using multiple bed load measurements: Toward the
 395 identification of bed dilation and contraction in gravel-bed rivers. *Journal of Geophysical*
 396 *Research*, 117(F1), F01014. <https://doi.org/10.1029/2011JF002120>
- 397 Masteller, C. C., & Finnegan, N. J. (2017). Interplay between grain protrusion and sediment
 398 entrainment in an experimental flume. *Journal of Geophysical Research: Earth Surface*,
 399 122(1), 2016JF003943. <https://doi.org/10.1002/2016JF003943>
- 400 Meyer-Petter, E., & Muller, R. (1948). Formulas for bed-load transport. In *Proceedings* (pp. 39–
 401 64). Stockholm, Sweden.
- 402 Paola, C., Heller, P. L., & Angevine, C. L. (1992). The large-scale dynamics of grain-size
 403 variation in alluvial basins, 1: Theory. *Basin Research*, 4, 73–90.
- 404 Paola, C., Straub, K., Mohrig, D., & Reinhardt, L. (2009). The unreasonable effectiveness of
 405 stratigraphic and geomorphic experiments. *Earth-Science Reviews*, 97(1–4), 1–43.
 406 <https://doi.org/10.1016/j.earscirev.2009.05.003>
- 407 Parker, G., & Wilcock, P. R. (1993). Sediment Feed and Recirculating Flumes: Fundamental
 408 Difference. *Journal of Hydraulic Engineering*, 119(11), 1192–1204.
 409 [https://doi.org/10.1061/\(ASCE\)0733-9429\(1993\)119:11\(1192\)](https://doi.org/10.1061/(ASCE)0733-9429(1993)119:11(1192))
- 410 Parker, G., & Wilcock, P. R. (1995). Closure to “Sediment Feed and Recirculating Flumes:
 411 Fundamental Difference” by Gary Parker and Peter R. Wilcock. *Journal of Hydraulic*
 412 *Engineering*, 121(3), 293–294. [https://doi.org/10.1061/\(ASCE\)0733-9429\(1995\)121:3\(293\)](https://doi.org/10.1061/(ASCE)0733-9429(1995)121:3(293))
- 413

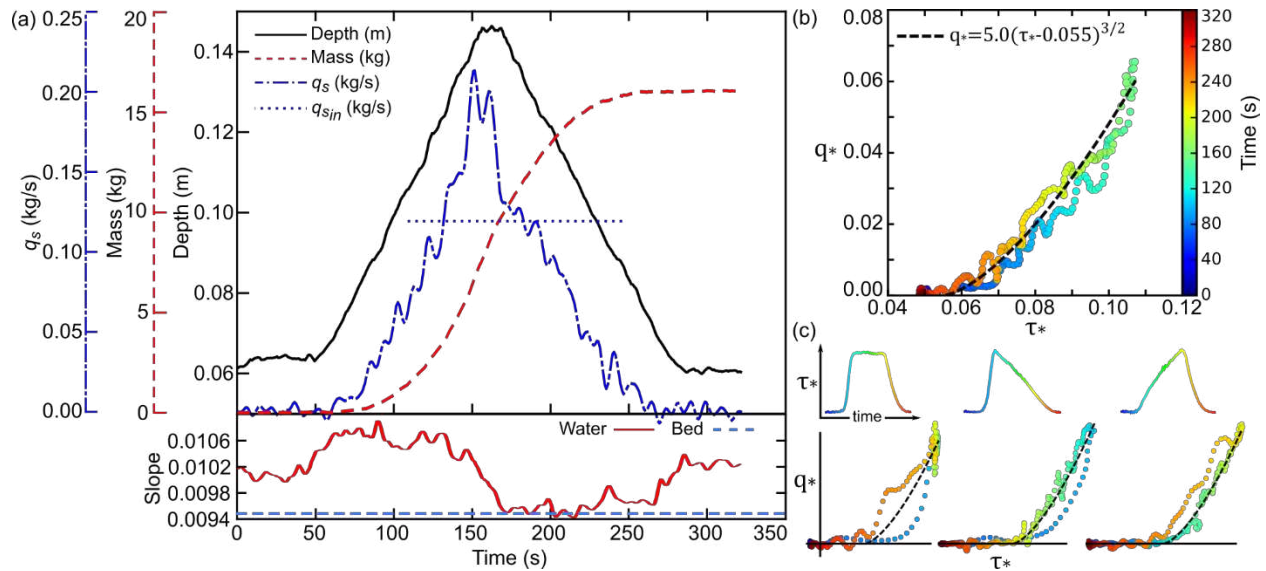
- 414 Parker, G., Hassan, M., & Wilcock, P. R. (2008). Adjustment of the bed surface size distribution
415 of gravel-bed rivers in response to cycled hydrographs. *Gravel-Bed Rivers VI: From*
416 *Process Understanding to River Restoration*, 241–285.
- 417 Phillips, C. B. (2018) Transient Flows Unimodal Sediment, SEAD Repository,
418 doi.org/10.5967/M0S180MK
- 419 Phillips, C. B., & Jerolmack, D. J. (2014). Dynamics and mechanics of bed-load tracer particles.
420 *Earth Surface Dynamics*, 2(2), 513–530. <https://doi.org/10.5194/esurf-2-513-2014>
- 421 Phillips, C. B., & Jerolmack, D. J. (2016). Self-organization of river channels as a critical filter
422 on climate signals. *Science*, 352(6286), 694–697. <https://doi.org/10.1126/science.aad3348>
- 423 Phillips, C. B., Martin, R. L., & Jerolmack, D. J. (2013). Impulse framework for unsteady flows
424 reveals superdiffusive bed load transport. *Geophysical Research Letters*, 40(7), 1328–
425 1333. <https://doi.org/10.1002/grl.50323>
- 426 Recking, A. (2012). Influence of sediment supply on mountain streams bedload transport.
427 *Geomorphology*, 175–176, 139–150. <https://doi.org/10.1016/j.geomorph.2012.07.005>
- 428 Recking, A. (2013). An analysis of nonlinearity effects on bed load transport prediction. *Journal*
429 *of Geophysical Research: Earth Surface*, 118(3), 1264–1281.
430 <https://doi.org/10.1002/jgrf.20090>
- 431 Reid, I., & Laronne, J. B. (1995). Bed Load Sediment Transport in an Ephemeral Stream and a
432 Comparison with Seasonal and Perennial Counterparts. *Water Resources Research*,
433 31(3), 773–781. <https://doi.org/10.1029/94WR02233>
- 434 Singer, M. B. 2010. Transient response in longitudinal grain size to reduced gravel supply in a
435 large river. *Geophysical Research Letters* 37: L18403, doi:18410.11029/12010gl044381,
436 10.1029/2010gl044381.
- 437 Singer, M. B., & Michaelides, K. (2014). How is topographic simplicity maintained in ephemeral
438 dryland channels? *Geology*, 42(12), 1091–1094. <https://doi.org/10.1130/G36267.1>
- 439 Strom, K., Papanicolaou, A. N., Evangelopoulos, N., & Odeh, M. (2004). Microforms in gravel
440 bed rivers: Formation, disintegration, and effects on bedload transport. *Journal of*
441 *Hydraulic Engineering-Asce*, 130(6), 554–567. [https://doi.org/10.1061/\(ASCE\)0733-
442 9429\(2004\)130:6\(544\)](https://doi.org/10.1061/(ASCE)0733-9429(2004)130:6(544))
- 443 Turowski, J. M., Badoux, A., & Rickenmann, D. (2011). Start and end of bedload transport in
444 gravel-bed streams. *Geophysical Research Letters*, 38, 5.
445 <https://doi.org/201110.1029/2010GL046558>
- 446 Vanoni, V. A., and N. H. Brooks (1975), *Sedimentation Engineering*. Manuals and Reports on
447 Engineering Practice No. 54, ASCE, 745, Am. Soc. Civ. Eng., Reston, Va.
- 448 Waters, K. A., & Curran, J. C. (2015). Linking bed morphology changes of two sediment
449 mixtures to sediment transport predictions in unsteady flows. *Water Resources Research*,
450 51(4), 2724–2741. <https://doi.org/10.1002/2014WR016083>
- 451 Whiting, P. J., & Stamm, J. (1995). The hydrology and form of spring-dominated channels.
452 *Geomorphology*, 12(3), 233–240. [https://doi.org/10.1016/0169-555X\(95\)00006-Q](https://doi.org/10.1016/0169-555X(95)00006-Q)
- 453 Wilcock, P. R. (1998). Two-Fraction Model of Initial Sediment Motion in Gravel-Bed Rivers.
454 *Science*, 280(5362), 410–412. <https://doi.org/10.1126/science.280.5362.410>
- 455 Wilcock, P. R., & Crowe, J. C. (2003). Surface-based Transport Model for Mixed-Size
456 Sediment. *Journal of Hydraulic Engineering*, 129(2), 120.
- 457 Wilcock, P. R., & McArdell, B. W. (1997). Partial transport of a sand/gravel sediment. *Water*
458 *Resources Research*, 33(1), 235–245. <https://doi.org/10.1029/96WR02672>

- 459 Wong, M., Parker, G., DeVries, P., Brown, T. M., & Burges, S. J. (2007). Experiments on
460 dispersion of tracer stones under lower-regime plane-bed equilibrium bed load transport.
461 *Water Resources Research*, *43*, 23. <https://doi.org/200710.1029/2006WR005172>
- 462 Wong, M., & Parker, G. (2006a). One-dimensional modeling of bed evolution in a gravel bed
463 river subject to a cycled flood hydrograph. *Journal of Geophysical Research*, *111*, 20.
464 <https://doi.org/200610.1029/2006JF000478>
- 465 Wong, M., & Parker, G. (2006b). Reanalysis and correction of bed-load relation of Meyer-Peter
466 and Muller using their own database. *Journal of Hydraulic Engineering-Asce*, *132*(11),
467 1159–1168. [https://doi.org/10.1061/\(ASCE\)0733-9429\(2006\)132:11\(1159\)](https://doi.org/10.1061/(ASCE)0733-9429(2006)132:11(1159))
- 468 Yager, E. M., Turowski, J. M., Rickenmann, D., & McArdell, B. W. (2012). Sediment supply,
469 grain protrusion, and bedload transport in mountain streams. *Geophysical Research*
470 *Letters*, *39*. <https://doi.org/10.1029/2012GL051654>
- 471 Zimmermann, A., Church, M., & Hassan, M. A. (2010). Step-pool stability: Testing the jammed
472 state hypothesis. *Journal of Geophysical Research: Earth Surface*, *115*(F2).
473 <https://doi.org/10.1029/2009JF001365>

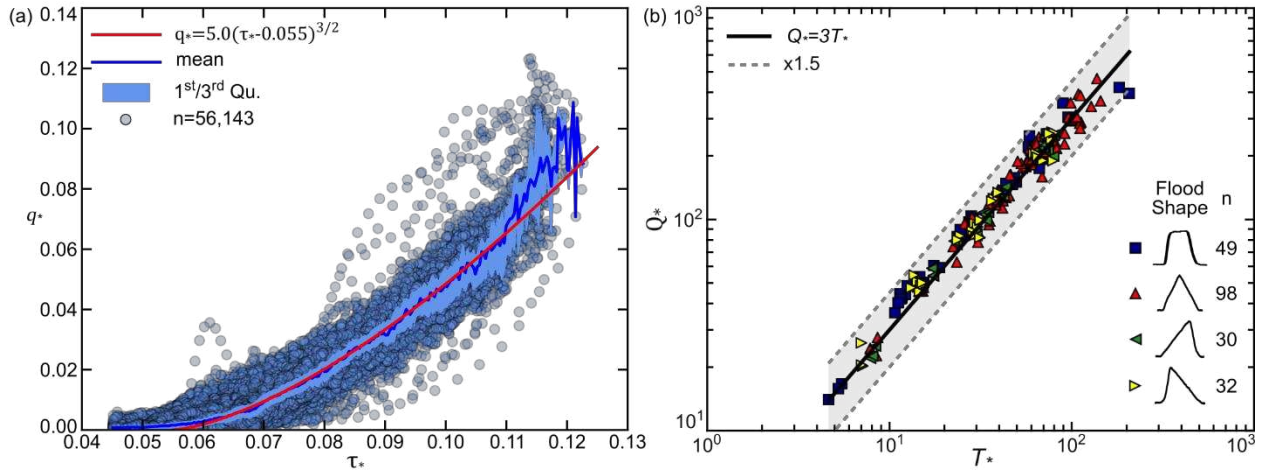


474
475
476
477
478
479
480
481
482
483
484

Figure 1. Experimental design. (a) Schematic hydrographs of steady (upper left) and unsteady (upper right) symmetric flows, and three unsteady flow shapes (lower left) explored in these experiments. (lower right) Schematic hydrographs showing two flows of equal impulse with different peak magnitude and duration. (b) Experimental parameter space of flow durations above the threshold of motion and dimensionless peak magnitude in shear velocity and shields stress normalized by the threshold of motion. Legend denotes experimental flood shape next to symbol. (c) Examples of experimental sequences. (top panel) Hydrograph sequence of steady and unsteady flows with equal peak magnitude and impulse for each run. (lower panel) Hydrograph of unsteady runs with alternating peak magnitude and duration.



485
 486 Figure 2. Experimental data. (a) Primary data are flow depth (black line), cumulative sediment
 487 mass (red dashed line), sediment feed rate (blue dotted line), and sediment flux (blue dash dot
 488 line). The subplot shows the water surface slope throughout the flood (red line) and the post
 489 flood bed surface slope (dashed line). (b) Dimensionless bed load flux and Shields stress for the
 490 run shown in (a), where color represents the experimental run time. The dashed black line
 491 represents a fitted bed load transport law. (c) Examples of flux stress relations for the other three
 492 flood shapes. The top row shows the flow hydrograph in time and stress with the color of the line
 493 corresponding to the approximate time location of the flux data in the bottom row. The bottom
 494 row shows sediment flux and Shields stress and the dashed black line represents the flux law in
 495 (b). For these schematic examples flux and stress are on the same scale for all three, while time is
 496 compressed by a factor ~ 1.3 for the asymmetric flood shapes.
 497



498
 499 Figure 3. (a) Dimensionless sediment transport rate and Shields stress for all experimental runs
 500 for $q_* \geq 0$ and $\tau_* \geq 0.045$. The blue line represents the average, shaded regions are the first and third
 501 quartiles, and the red line is the fitted sediment transport flux law. (b) Dimensionless impulse
 502 (T_*) versus dimensionless cumulative sediment flux (Q_*) for all runs. Example hydrographs for
 503 each run are depicted next to the symbols alongside the number of runs for that flood shape. The
 504 black line is a linear trend line fit through the origin, and the grey dashed lines represent a factor
 505 of 1.5 times the linear trend.